Effects of galvanometer laser scanning system on the structural integrity of 3D printed parts.

By
Charles Bibas
Tecnica, Inc.

Abstract

3D Selective Laser Sintering (SLS) and Selective Laser Melting (SLM) Printers create parts by rendering multiple 2D layers to create 3D parts. The only effective way to create high-definition parts is to deliver constant energy through a beam targeted at the print surface. For the past 30 years, SLS and SLM 3D printing companies have been using galvanometers to focus the beam. The galvanometer mechanism involves the use of a pair of oscillating mirrors via objective lenses that need to focus the beam at a constant distance. However, since the beam is moving back and forth, the distance from the beam to the print surface is constantly changing, causing a variable change in the amount of energy hitting its target at every point. Additionally, the beam location accuracy error grows as the beam moves away from the center. The uneven distribution of energy results in the low-resolution prints we have today. Four significant errors are found in traditional 3D SLS/SLM printers using galvanometers. As the mirrors rotate to deflect the beam, there are evident changes in the beam diameter, shape, speed, location and decrease of output energy. The combination of these non-linear errors increases in magnitude as the beam moves farther from the center and closer to the print edge. 3D printers using galvanometers must use f-theta lenses to maintain a constant speed between laser dots. While this method mitigates some of the print distortions, it does not resolve the other issues described above. In addition, the work area build size is limited by the physical size constraints of the lenses. To address the inherent problems with galvanometers and associated lens systems, Tecnica developed a revolutionary, patented technology that eliminates traditional scanning errors. This paper quantifies the shortcomings of existing systems and apprises the readers of Tecnica's technology.

Table of Contents

Introduction 4

Types of errors 5

Differential laser scan speed 5

Differential energy absorption 6

Differential laser beam shape 6

Out-of-focus incidence for laser beam 8

Results 12

Conclusion 15

Appendix: Correction lenses for traditional solutions 16

References 17

Introduction

Θ (capital theta) is defined as the instantaneous angle between the normal to target plane and the laser beam. As seen from Fig.1, Θ increases as the rotating mirror oscillates away from the mean position to reflect the beam away from the surface normal. This results in a differential cross-sectional area for the laser beam, a gradual transition to an ellipsoidal-like cross-section from a circular.

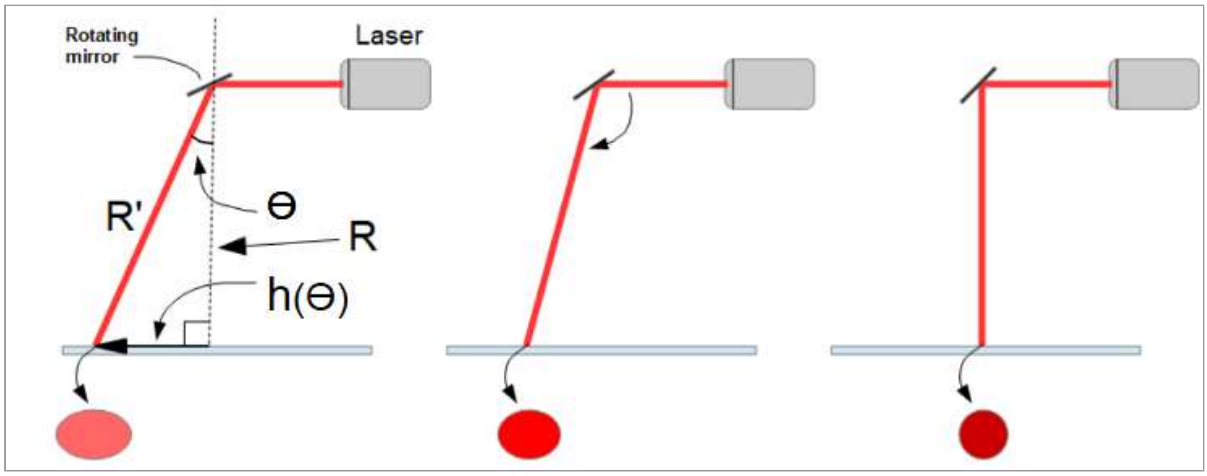

Fig 1. Schematic of a scanning system.

It is important to note that incident angle Θ is not a measure of deflection of a galvanometer but a measurement at the surface. Furthermore, the scanning angle Θ is numerically twice the deflection angle of the galvanometer. Thus, for a typical galvanometer deflection angle of ±14°, the dynamic FOV angle at the surface is ±28°.

The following sections discuss in detail various types of errors encountered with the use of oscillating mirror setup in galvanometers.

Types of errors

Typical errors encountered in 3D printers based on a galvanometer and a lens system can be categorized as:

1. Differential laser scan speed
2. Differential energy absorption
3. Differential laser beam shape
4. Out-of-focus incidence for laser beam

1. Differential laser scan speed

Consider a rotating mirror positioned at the center of a circle with radius R as seen in Fig.1. As the mirror gradually rotates, the reflected laser beam travels linearly onto the target plane with velocity V_0. This linear velocity V_0 is expressed as,

$$V_0 = \omega \times R$$

where ω is the angular velocity and defined as the time rate of change of Θ (Θ = ω x t).
The beam travels a distance h from the initial start point (origin) as a result, which can be expressed as,

$$h = R \times \tan(\Theta)$$

As the mirror rotates further, with proportional increases in Θ, the endpoint of the laser beam is no longer R distance away from the origin but is now defined by the time rate of change of h.
Instantaneous linear velocity V can then be calculated as:

$$V(t) = dh/dt = Vo \times 1/cos^2(\omega \times t) \quad (1)$$

Θ	***V***
π/4	$V_0 \times 2$
π/8	$V_0 \times 1.17$
π/16	$V_0 \times 1.03$

Table 1. Summary of test values for instantaneous linear velocity *V*.

The expression for instantaneous velocity *V* indicates that velocity is inversely proportional to the cosine of incident angle Θ, as is evident from the data in Table 1. Also, the incident energy per unit time is inversely proportional to scan speed *V*. The beam, therefore, delivers less energy as it moves away from the mean position with a proportional increase in travel speeds as it spends less time on the scan area.

2. Differential energy absorption

From Lambert's cosine law, energy absorbed by a surface is proportional to the cosine angle included between the striking beam angle and the normal.

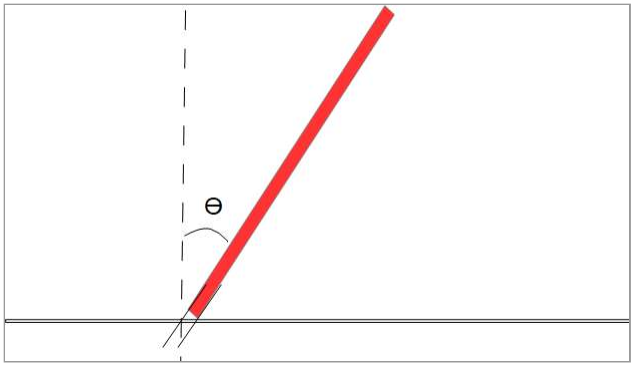

Fig 2. The incidence angle of laser beam striking angle Θ.

Energy *E(Θ)* absorbed by work surface in unit time *T* is then quantified as:

$$E(\omega\, x\, t) = E_0 \cdot \cos(\omega\, x\, t) \quad (2)$$

Alternatively, expressed with Θ as:

$$E(\Theta) = E_0 \cdot \cos(\Theta) \quad (2)$$

where E_0 is the intensity of the incident beam when the beam is normal to the surface.

As evident from equation (2), the amount of laser energy delivered to the work surface decreases as Θ increases. This decreased energy input on feedstock material leads to partial sintering and thereby poor inter-layer adhesion.

3. Differential laser beam shape

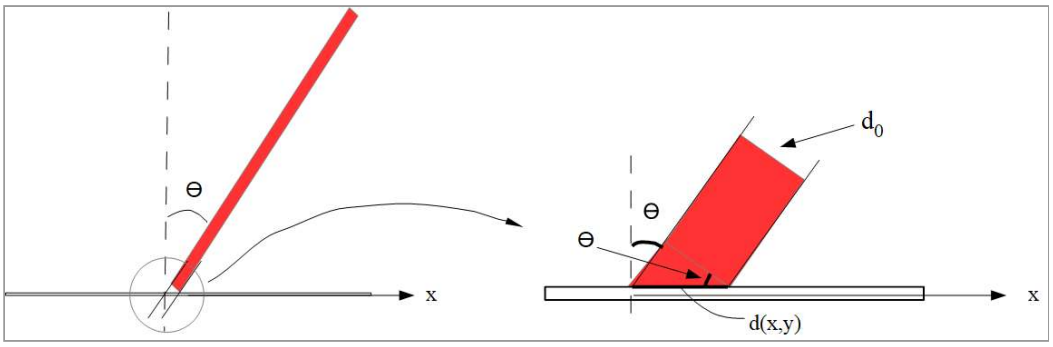

Fig. 3 Beam shape and size change as Θ changes.

Assume a collimated circular beam with beam diameter d_0 striking normally to the work surface. As seen from Fig.3, the beam cross-section is no longer circular as Θ increases. The circular cross-section progressively evolves into an ellipse defined by d_x and d_y.

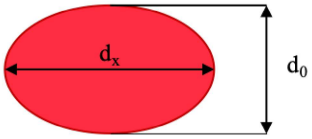

Fig. 4 Elliptical cross-section of the laser beam on the worksurface using one Galvanometer on the x-axis.

Major axis d_x can be expressed as:

$$d_x = d_0/\cos(\Theta)$$

Cross-sectional area A of elliptical laser beam shown in Fig. 4 can be expressed as,

$$A = Pi^2/4 \times d_x \times d_0$$

$$A = Pi^2/4 \times d_0^2 \times 1/\cos(\Theta)$$

$$\boldsymbol{A = A_0 \times 1/\cos(\Theta)} \qquad (3)$$

where $\boldsymbol{A_0}$ is the area of the circular cross-section of diameter d_0.

Note: For simplicity, error in consideration assumes differential changes along the X-axis. Similar errors occur also along the Y-axis (second galvanometer) distorting the initial circular cross-section of the laser beam into an ellipse. Moreover, as the galvanometer mirrors rotate about the X and Y axes,

the distortion of the circular cross-section to the ellipse is the vector sum of the distortion along each axis. There will be additional 2D distortion (barrel distortion) within the galvanometers.

Differential beam shape, coupled with increased scan speeds as discussed previously, leads to decreased incident energy. This incident energy can be divided into two components – a horizontal component for build plane sintering and a vertical component for interlayer bonding. This results in:

1. Inconsistent interlayer bonding
2. Decreased resolution
3. Porosity

4. Out-of-focus incidence for laser beam

As the mirror oscillates back and forth to direct the laser beam, it moves the focal point on a circle[1] whose radius is defined by focal length. As seen in Fig. 5, the laser beam strikes the work surface out of focus as the mirror reflects the beam away from the mean position.

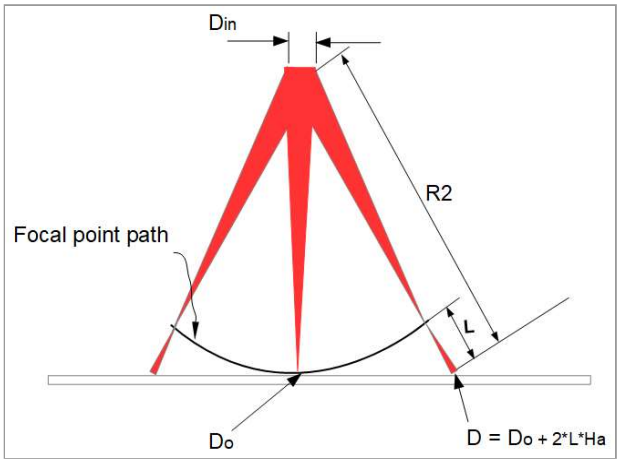

Fig. 5 – Schematic showing focal point path.

Beam diameter size along the optical path is dictated by the beam Half-angle (Ha) divergence or convergence angle and defined as the sine of expanding half-angle of the beam. The enlarged out-of-focus diameter *D* of the incident laser beam can be expressed as,

$$D = D_0 + 2 \times L \times Ha$$

[1]This analysis assumes no scanning in the Y direction of the coordinate system. The focal point lies on a torodial when scanning with both Galvanometers.

where D_0 is the beam diameter at-focus and L = R2 - R.

R2 is the beam distance from the mirror to the work surface as the beam travels away from the initial start point as seen in Fig. 5.

$$D = D_0 + 2 \times R \times (1/\cos(\Theta) - 1) \times Ha \quad (4)$$

Off Sphere Constant (OSC) can be defined as the ratio of out-of-focus beam diameter to in-focus beam diameter and is expressed as,

$$OSC(\Theta) = D \div D_0$$

$$= 1 + 2 \times R \times (1/\cos(\Theta) - 1) \times Ha \div D_0 \quad (5)$$

Specifications data from a typical powder bed fusion machine manufacturer suggests an approximate value of 1.5 for OSC and it varies as a function of R, Ha, and Θ.

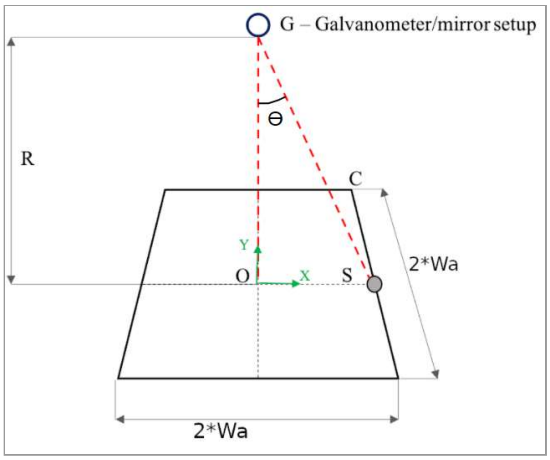

Fig. 6 - Schematic of laser incidence from galvanometer to print bed.

Output beam diameter at focus = *Do*

Input beam diameter at galvanometer mirror = D_{in}

$$D_0 = D_{in} - 2 \cdot R \cdot Ha$$

$$\therefore Ha = (D_0 - D_{in})/(2 \cdot R)$$

From Fig. 6, $\tan(\Theta) = Wa / R = K$

Substituting the above expressions in Eq. (4) where Ha is substituted with -Ha,

$$D = Do + (D_{in} - D_0) \cdot (1/\cos(\arctan(K)) - 1)$$

Fig. 7 shows a graph of the equation above with Do = 0.1 mm.

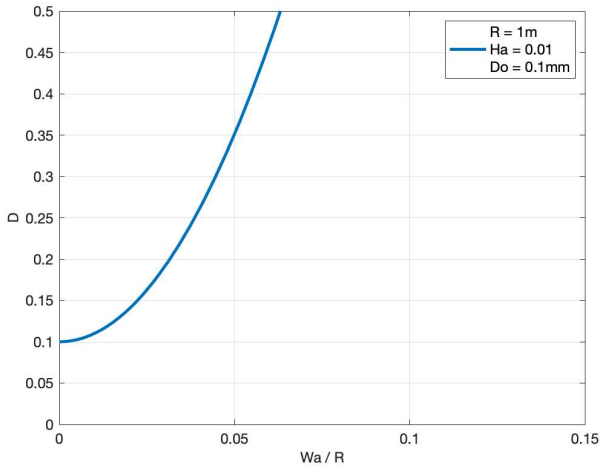

Fig. 7 - Effect of distance between galvanometer and print bed on laser beam diameter.

As seen from Fig. 7, the cross-section area of the beam striking the work surface increases dramatically as K increases. As K represents the ratio of bed size to R (Wa/R), it demonstrates clearly that R needs to be relatively large in comparison to the print bed to keep the beam diameter distortion to a minimum

The following example provides a quantitative perspective on shortcomings on the use of galvanometers and the need for a sound solution.

E.g. –

Input beam diameter D_{in} = 5 mm

Output beam diameter D_0 = 0.1mm

Assume a print bed area of 300 x 300 mm^2 with the galvanometer setup positioned symmetrically at a distance R = 2 m as shown in Fig. 8.

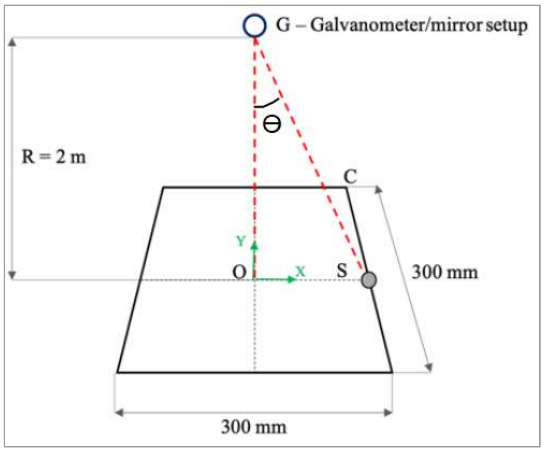

Fig.8 - Schematic of laser incidence from galvanometer to print bed.

Assume that the beam needs to strike a point midway through any one of the sides of the print bed denoted by point S in Fig. 6. In this event, the scanning angle Θ can be found using trigonometry as:

$$\tan(\Theta) = 0.15 \div 2$$

$$\therefore \Theta = 4.2°$$

Ha can be calculated using the expression:

$$D_{in} = 2 \times Ha \times R \times D_0$$

Substituting values for D_{in}, R, and D_0

$$Ha = 0.0125$$

Using Eq. (4), out-of-focus diameter D = 0.235 mm.

Print resolution is reduced to half since the beam diameter is more than doubled to 0.235 mm from its initial in-focus diameter of 0.1 mm.

Consider the case where the beam strikes point C in Fig. 8. The effective radius of the beam can be resolved as:

$$R_C^2 = R^2 + (\sqrt{2} \times 0.15)^2$$

$$R_C = 2.011 \text{ m}$$

Using trigonometry, the effective angle of inclination Θ is:

$$\text{Tan}(\Theta) = \sqrt{2} \times 0.15 \div 2$$

$$\therefore \Theta = 6.07°$$

Using Eq. (4), out-of-focus diameter at point C: $D_c = 0.438$mm.

Print resolution is severely affected since the beam diameter is more than tripled to 0.438mm from an initial in-focus diameter of 0.1 mm. This indicates that an increase in beam inclination Θ, as well as an increase in effective radius R, has adverse effects on print resolution.

One of the ways to mitigate this particular error is to use large values for R relative to the print size. Higher values for R indicate more travel on the print bed achieved with comparatively lesser rotation of the galvanometer, i.e. Θ for the projected beam. Increase in out-of-focus beam diameter D is restricted since it is inversely proportional to cosine (Θ). However, the increase in R also results in increased physical dimensions of the printer and sensitivity to vibrations. Furthermore, when the beam is directed at off-axis points, say point C, field of view angle Θ is now the vector sum of

inclinations on X and Y axis. This results in larger values for Θ as well as increased effective radius R, both adding to increased distortion of the incident beam as evident from the previous example.

Results

As discussed, galvanometer systems have inherent problems in their mechanisms that lead to heterogeneities in the build part. Table 2 provides an overview of errors discussed previously. For conciseness, error numbers designated in the first column correspond to respective error descriptions provided earlier. For simplicity, errors along X-axis are summarized in Table 2 and it is expected that errors along Y follow a similar trend.

Error	Resolution	Scan speed	Beam Size	Energy Absorption
1	Unchanged	Increased	Unchanged	Decreased
2	Decreased	Unchanged	Increased	Decreased
3	Decreased	Unchanged	Increased	Decreased
4	Decreased	Unchanged	Increased	Decreased

Table 2 – Summary of errors occurring in a galvanometer system.

Energy *E,* can be expressed in terms of power *P* and time *T* as,

$$E = \mathrm{P} \times \mathrm{T}$$

Energy density E_d, defined per unit area, can be expressed as,

$$E_d = \mathrm{E} \div \mathrm{A2}$$

where A2 is an area of a single rectangular track deposited by a beam of diameter *d* with velocity *V* and travel time *T* time and is expressed as,

In 3D printing, energy density is expressed by either the use of hatch distance [14] or using the beam diameter [15]. Using the beam diameter method [15], the energy density is expressed by:

$$E_d = \frac{P}{d \times V} \tag{6}$$

From errors in galvanometer scanning discussed in previous sections, the beam diameter *d,* velocity *V*, and incident power *P* change. Substituting eq (6) with eq (1), (2), (3), (6) as illustrated in Fig. 9

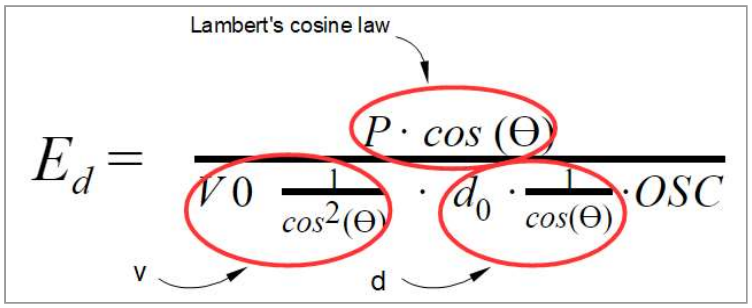

Fig. 9

$$E_d = \frac{P \cdot \cos(\Theta)}{V0 \frac{1}{\cos^2(\Theta)} \cdot d_0 \cdot \frac{1}{\cos(\Theta)} \cdot OSC} = \frac{P \cos^4(\Theta)}{V0 \times d_0 \times OSC} \quad (7)$$

where V_0 is constant.

Eq. (7) can be expressed as a function of deflection angle Θ and OSC as:

$$E_d = \frac{Eo \cos^4(\Theta)}{OSC} \quad (8)$$

where $E_0 = \frac{P}{V0 \times d}$ for $1 < OSC < 2$

Even if we assume that OSC is 1; indicating that the beam is keeping its focus across the work area. Then the energy density is estimated to be:

$$E_d = E_0 \cdot \cos^4(\Theta) \quad (9)$$

Figure 10 shows a plot for Eq. (9) for two different values of OSC viz, 1 and 1.5. The unit value for OSC indicates an ideal situation where the beam diameter would not increase due to out-of-focus incidence. However, the energy density still changes as a function of deflection angle Θ as seen from Fig. 10. OSC of 1.5 is a typical value reported in speciation data for contemporary 3D SLS/SLM printer manufacturers.

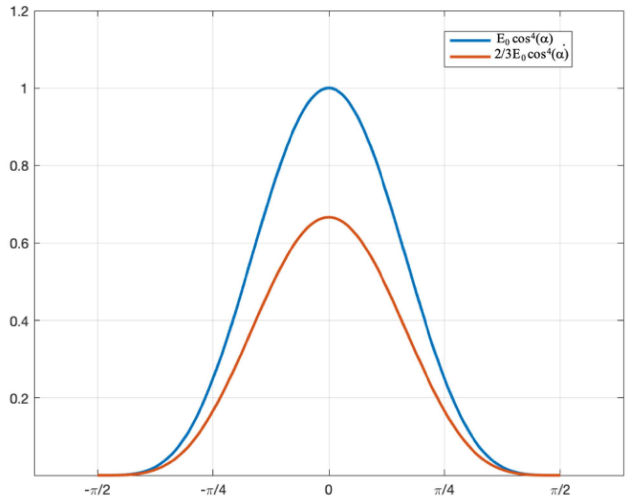

Fig. 10 – Plot for energy density for different OSC.

As observed from the graph, energy density decreases dramatically as Θ deviates from the mean position. Furthermore, the energy density for the graph with an OSC of 1.5 is less compared to energy density for a unit OSC regardless of Θ. A higher value for OSC indicates an increased possibility of considerably less amount of energy available for sintering.

As evident from results, inclination angle Θ governs various processing parameters, including beam cross-section, scan speeds, and energy density among others. Table 2 below summarizes errors introduced as the galvanometer directs the incoming laser beam at various angles of inclination Θ. It is important to note that errors discussed throughout the paper were constrained to one axis, say X, on the X-Y coordinate system. Similar errors will be observed for measurements on the Y-axis with the total error being the vector sum of individual errors.

Parameter	**22° ≤ Θ >11°**	**11° ≥ Θ > 0°**	**~ 0°**
Beam cross-section	Severe distortion	Distortion	✓
Resolution	Severe distortion	Distortion	✓
Scan speed	Increases exponentially proportional to $1/Cos^2(\Theta)$	Increases exponentially proportional to $1/Cos^2(\Theta)$	✓
Energy density	Decreases exponentially proportional to $Cos^4(\Theta)$	Decreases exponentially proportional to $Cos^4(\Theta)$	✓

Table 3 - Summary of errors introduced in a traditional Galvanometer based system.

As seen from Table 3, distortions grow dramatically as Θ increases beyond the 11° - 22° range.

In order to mitigate the Θ errors, the movement of the mirrors in the galvanometer is restricted, resulting in underutilization of the scanning system. Furthermore, limiting inclination for the laser beam leads to a decreased print area since the beam can now not be directed further away from the mean position.

Conclusion

As reported, traditional scanning systems have inherent problems directing a laser beam onto the target plane. The use of galvanometer systems leads to discrepancies such as differential cross-sectional area of the beam, non-normal incidence, increased scan speeds, and decrease in energy deposition. The use of F-theta lenses and offset-mapping software can mitigate these problems only to a limited extent.

Tecnicas' technology completely eliminates the errors associated with the use of the galvanometer system. Tecnica3D™ uses two mirrors, where one mirror is stationary and the other constantly rotating to direct the incoming laser beam onto the print bed. Since there is no oscillating mechanism, the incident beam is always in focus and normal to print the surface. With Tecnica3D™, the laser beam does not suffer from any lens aberrations or loss of energy density as the system is lens-free.

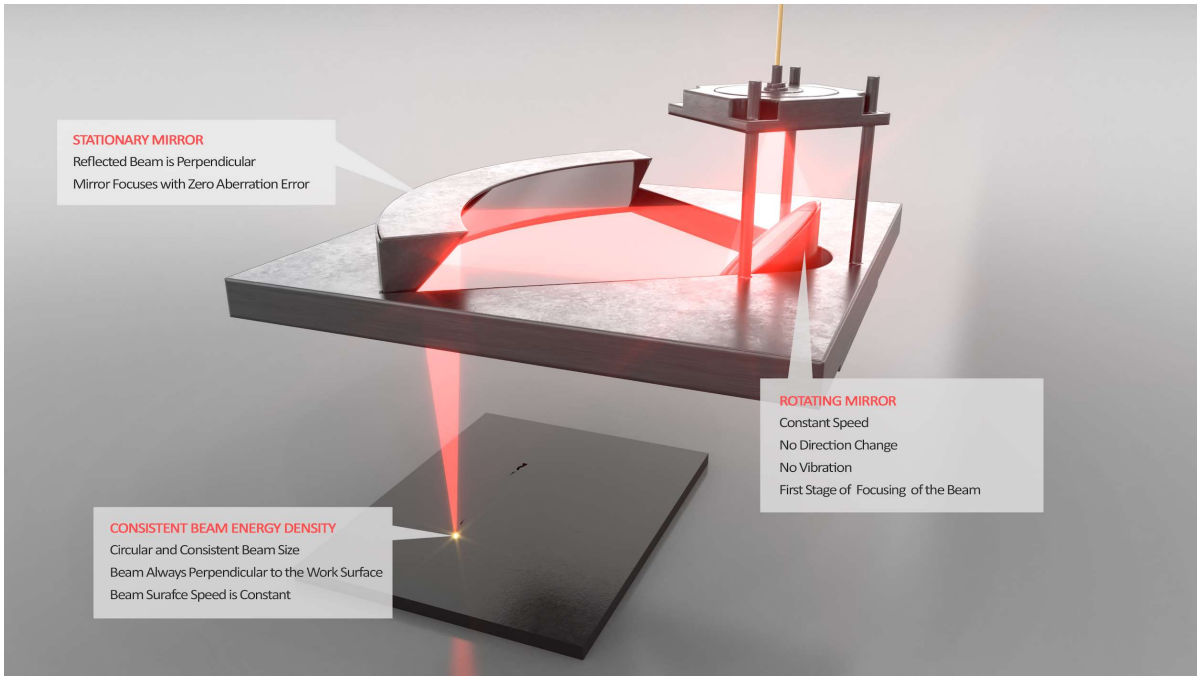

Fig. 11 - Tecnica3D illustration - Protect under multiple patents

Tecnica3D™ surpasses the performance of the galvanometer-based system in terms of scan speed. Furthermore, Tecnica3D™ use of mirrors instead of a scanning lens makes the system more scalable, because mirrors have few manufacturing constraints compared to lenses. With Tecnica3D™, the incidence of the laser beam is always normal to the print bed regardless of the target point. This ensures uniform energy input to each powder particle on the bed for proper fusion, thus improving structural integrity and dimensional accuracy of the building part.

Appendix: Correction lenses for traditional solutions

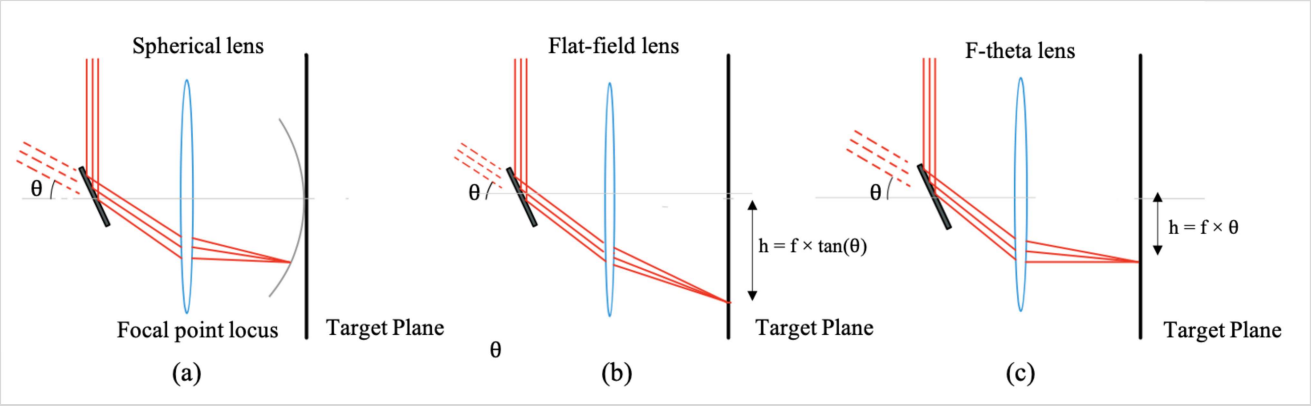

Fig. 12 – Types of lenses.

Distortion is introduced in an optical system where the image height *h2* is not linearly proportional to the scanning angle. In such a system, the image height *h2* is proportional to tan (Θ) and expressed as:

$$h2 = f \times \tan(\Theta)$$

where f is the focal length and is the angular angle.

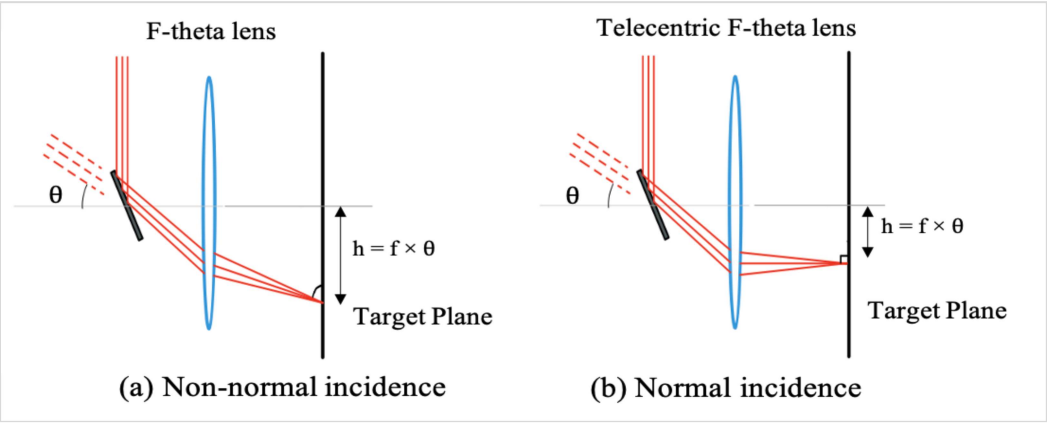

Fig. 13 – Typical correction lenses uses in traditional SLS/SLM 3D printers.

F-theta lenses have been developed to mitigate the problem of non-linearity in spot positioning with weak aberrations. The spot position for F-theta is roughly the product of *f* and Θ, unlike flat-field lenses. Telecentric lenses facilitate normal incidence of laser beam onto the target plane as seen in Fig. 13 (b) However, a major disadvantage of the telecentric lens is that the scannable area is limited by lens size. Hence, these lenses cannot be used to produce normal incidence over the large print area desirable in 3D printing applications.

References

[1] Fabbaloo.com - Why are 3D printers so tall?

[2] RP-Photonics – Scanning lenses.

[3] B. P. Conner, G. P. Manogharan, A. N. Martof et al., "Making sense of 3-D printing: Creating a map of additive manufacturing products and services," Additive Manufacturing, vol. 1, no. 4, pp. 64-76, 2014.

[4] K. V. Wong and A. Hernandez, "A review of additive manufacturing," International Scholarly Research Network (ISRN) Mechanical Engineering, 2012.

[5] D. Faidel, A. Laskin, W. Behr, and Natour, "Improvement of selective laser melting by beam shaping and minimized thermally induced effects in optical systems," in Proc. 9th International Conference on Photonic Technologies, 2016.

[6] Q. Zhao, C. Wang, and J. H. Yang, "Graphic distortion analysis and correction arithmetic research on laser galvanometer scanning," Journal of Changchun University of Science and Technology, vol. 35, no. 4, pp. 63-75, 2012.

[7] C. K. Zhu and L. P. Ding. "Research on forming qualities during selective laser melting based on scanner delay strategy," Applied Laser, vol. 37, no. 2, pp. 207-212, 2017.

[8] X. Luo, J. Li, and M. Lucas, "Galvanometer scanning technology for laser additive manufacturing," Proceedings of SPIE, Vol. 10095, 2017.

[9] G. Y. Li, Y. Z. Wang, J. R. Han, and S. Y. Liu, "Geometry algorithm of galvanometer system correction for rapid prototyping of machine parts," Machine Tool & Hydraulics, vol. 42, no. 19, pp. 28-30, 2014.

[10] Q. Zhao, C. Wang, and J. H. Yang, "Graphic distortion analysis and correction arithmetic research on laser galvanometer scanning," Journal of Changchun University of Science and Technology, vol. 35, no. 4, pp. 63-65. 2012.

[11] H. W. Yoo, S. Ito, and G. Schitter, "High speed of laser scanning microscopy by iterative learning control of a galvanometer scanner," Control Engineer Practice, vol. 50, pp. 12-21, 2016.

[12] Huang Jigang, Qin Qin, Wang Jie, and Fang Hui - Two-Dimensional Laser Galvanometer Scanning Technology for Additive Manufacturing. International Journal of Materials, Mechanics and Manufacturing, Vol. 6, No. 5, October 2018

[13] Design of Large Working Area F-Theta Lens Gong Chen optics.arizona.edu/sites/optics.arizona.edu/files/msreport-gong-chen.pdf

[14] Bai, S.; Perevoshchikova, N.; Sha, Y.; Wu, X. The Effects of Selective Laser Melting Process Parameters on Relative Density of the AlSi10Mg Parts and Suitable Procedures of the Archimedes Method. *Appl. Sci.* **2019**, *9*, 583. https://doi.org/10.3390/app9030583

[15] Metel, A.S.; Stebulyanin, M.M.; Fedorov, S.V.; Okunkova, A.A. Power Density Distribution for Laser Additive Manufacturing (SLM): Potential, Fundamentals and Advanced Applications. Technologies 2019, 7, 5. https://doi.org/10.3390/technologies7010005